University of Glasgow

Connell, A. et al. (2019) Low cost triazatruxene hole transporting material for >20% efficient perovskite solar cells. *Journal of Materials Chemistry C*, 7, pp. 5235-5243. (doi:10.1039/C8TC04231D)

This is the author's final accepted version.

There may be differences between this version and the published version. You are advised to consult the publisher's version if you wish to cite from it.

http://eprints.gla.ac.uk/173162/

Deposited on: 16 November 2018

Enlighten – Research publications by members of the University of Glasgow
http://eprints.gla.ac.uk

Check for updates

View Article Online
View Journal

Journal of Materials Chemistry C

Accepted Manuscript

This article can be cited before page numbers have been issued, to do this please use: A. Connell, Z. Wang, Y. Lin, P. Greenwood, A. wiles, E. Jones, L. Furnell, R. Anthony, C. Kershaw, G. Cooke, H. Snaith and P. J. Holliman, *J. Mater. Chem. C*, 2018, DOI: 10.1039/C8TC04231D.

This is an Accepted Manuscript, which has been through the Royal Society of Chemistry peer review process and has been accepted for publication.

Accepted Manuscripts are published online shortly after acceptance, before technical editing, formatting and proof reading. Using this free service, authors can make their results available to the community, in citable form, before we publish the edited article. We will replace this Accepted Manuscript with the edited and formatted Advance Article as soon as it is available.

You can find more information about Accepted Manuscripts in the author guidelines.

Please note that technical editing may introduce minor changes to the text and/or graphics, which may alter content. The journal's standard Terms & Conditions and the ethical guidelines, outlined in our author and reviewer resource centre, still apply. In no event shall the Royal Society of Chemistry be held responsible for any errors or omissions in this Accepted Manuscript or any consequences arising from the use of any information it contains.

ROYAL SOCIETY OF CHEMISTRY

rsc.li/materials-c

View Article Online
DOI: 10.1039/C8TC04231D

Low cost triazatruxene hole transporting material for >20% efficient perovskite solar cells

Arthur Connell,†[a] Zhiping Wang,†[b*] Yen-Hung Lin,[b] Peter C. Greenwood,[a] Alan A. Wiles,[c] Eurig W. Jones,[a] Leo Furnell,[a] Rosie Anthony,[a] Christopher P. Kershaw,[a] Graeme Cooke,[c] Henry. J. Snaith,[b*] and Peter J. Holliman,[a*]

[a] College of Engineering, Bay Campus, Swansea University, Swansea, SA1 8EN, UK

[b] Department of Physics, University of Oxford, Clarendon Laboratory, Parks Road, Oxford OX1 3PU, UK

[c] Glasgow Centre for Physical Organic Chemistry (GCPOC), WestCHEM, School of Chemistry, University of Glasgow, Glasgow, G12 8QQ, UK

*Corresponding authors: (Z.W.) zhiping.wang@physics.ox.ac.uk; (H.J.S.) henry.snaith@physics.ox.ac.uk; (P.J.H.) p.j.holliman@swansea.ac.uk.

† These authors contributed equally to this work.

Published on 15 November 2018. Downloaded by University of Glasgow Library on 11/16/2018 11:25:17 AM.

Journal of Materials Chemistry C Accepted Manuscript

ABSTRACT: Organic hole-transporting materials (HTM) have shown excellent ability in achieving high efficiency perovskite solar cells. However, their high cost significantly limits their applications in scaling-up perovskite solar cells. Here, we report an efficient, low-cost HTM, called TAT-^{t}BuSty, comprising a central triazatruxene moiety with 3 terminal *tert*-butoxy styrene groups and 3 hexyl side chains on the indole nitrogen. For the first time, we use an inexpensive liquid precursor to attach the donor ligand to the molecule. This enables purification of the HTM using a silica plug and recrystallization without the need for complicated column chromatography, which is typically required to purify solid-precursor-prepared HTMs. We estimate that the cost for the purified TAT-^{t}BuSty is \$69.90 g^{-1}, which is 35% cheaper than the widely-used 2,2′7,7′-tetrakis-(*N*,*N*-di-*p*-methoxyphenyl-amine)-9,9′-spirobifluorene (spiro-OMeTAD; *ca.* \$112.05 g^{-1}). Using this low-cost TAT-^{t}BuSty as the HTM in a caesium-formamidinium mixed-cation perovskite solar cell, we have successfully achieved a champion power conversion efficiency (PCE) of 20.3% (19.4% stabilized efficiency), which is comparable to the efficiency of devices using the reference spiro-OMeTAD HTM. Our work is crucial for up-scaling of next-generation high-performance metal-halide perovskite solar cells.

Introduction

Metal-halide perovskite solar cells (PSCs) have attracted huge interest to the academic and industrial community because of their meteoric rise in efficiency[1–10]. Due to continuous improvements of perovskite formulations and deposition methods, the record efficiency has reached a certified value of 23.3%[11]. Most of the high efficiency devices, especially the negative-

View Article Online
DOI: 10.1039/C8TC04231D

Published on 15 November 2018. Downloaded by University of Glasgow Library on 11/16/2018 11:25:17 AM.

intrinsic-positive (n-i-p) structured devices, use 2,2′7,7′-tetrakis-(*N,N*-di-*p*-methoxyphenyl-amine)-9,9′-spirobifluorene (spiro-OMeTAD) and polytriarylamine (PTAA) as the HTM. However commercially available spiro-OMeTAD costs over \$150 g^{-1} and PTAA is more than twice the cost of spiro-OMeTAD. The high cost makes it difficult to apply these materials for scaling-up fabrication. One reason for this is that the synthesis of spiro-OMeTAD requires 6 steps from expensive precursors and sophisticated purification processes to attain the high quality[12]. At the same time, preparation of well-defined, high molecular weight PTAA is particularly demanding as the step-growth polymerisation requires exact stoichiometry and very high conversion of the functional groups to achieve good yields of polymeric material[13]. Hence, the development of low-cost, scalable HTMs without sacrificing device efficiencies is highly desired to improve the progress of PSCs towards commercialization.

In this work, we have synthesized a low-cost and efficient triazatruxene (TAT) HTM for use in PSC devices. We chose triazatruxene (Fig. 1) as the central core of TAT-^{t}BuSty because it can be prepared at low cost from precursors synthesized from highly abundant natural products. In addition, TAT is synthetically versatile with reactive sites on the indole N atoms and benzene rings enabling tuning of the optical, electronic and morphological properties. Furthermore, the 3 nitrogen atoms of each indole unit should help stabilize the radical cation of the oxidized HTM during device operation. Finally, the rigid planar molecular structure could help to improve the materials resistance to photo and thermal degradation as seen in other discotic mesogens such as phthalocyanine pigments. We have derivatized the triazatruxene core by attaching hexyl chains to reactive site 1 and replacing the commonly used dimethoxydiphenylamine or anisole donors with a much cheaper *tert*-butoxystyrene moiety at reactive site 2. Attaching dimethoxydiphenylamine or anisole donors to the triazatruxene central unit requires solid precursors which are reacted with a solid central core to form a solid product. Purification of a HTM with precursors in this form requires complicated column chormatography to separate unreacted solid starting materials. In contrast, we attach *tert*-butoxystyrene to the triazatruxene central unit which involves reaction of the cheap liquid precursor (*tert*-butoxysryrene) to the triazatruxene central core. This synthetic strategy of reacting a liquid with a solid to form the solid HTM product avoids the need for purification using complicated column chromatography which decreases cost by hugely decreasing solvent usage and operator time. The *tert*-butoxystyrene can be added in excess and recycled at the end of the reaction. To the best of our knowledge, this is the first time that *tert*-butoxystyrene has been used as a donor ligand in any HTM and it is also the first report focusing on a synthetic strategy to decrease cost and environmental imapact when synthesizing organic HTMs instead of just

Journal of Materials Chemistry C Accepted Manuscript

View Article Online
DOI: 10.1039/C8TC04231D

focusing on starting material and reagent costs. TAT-^{t}BuSty can be synthesized for 24% less than the cost of the next best performing triazatruxene, SP12 as shown in S4 (ESI) and for 35% less than spiro-OMeTAD[12]. This new HTM has been fully characterised, and its performance tested in PSC devices giving a high power conversion efficiency (PCE) of 20.3%.

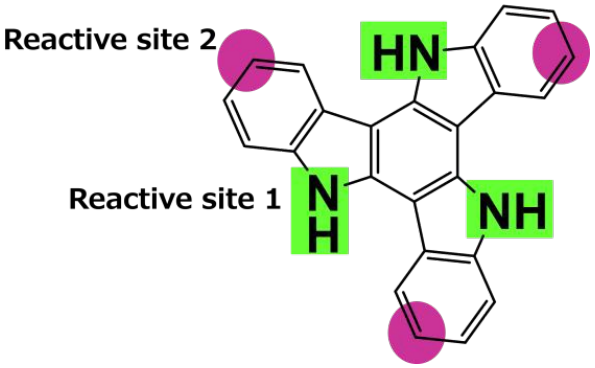

Figure 1. Triazatruxene (TAT) molecular structure with reactive sites highlighted.

Results and Discussion

Synthesis

Triazatruxene **(2)** is initially formed by cyclisation of oxindole **(1)** using $POCl_3$ as described by Rakstys *et al.*[14] and Su *et al.*[15]. The data are in line with published reports (S1 ESI) and this is a moderate yield (65%) reaction which is neutralized in ice water with NaOH yielding **(3).** This is followed by two reactions which occur in 75 and 82% yield; first, the alkylation of the indole nitrogen atoms with iodohexane and then bromination of the benzene rings using N-bromosuccinimide (NBS) to produce **(4)**. Finally, TAT-^{t}BuSty **(5)** was prepared using a Pd-catalysed Heck coupling to attach three *tert*-butoxy styrene donor ligands to the benzene rings of the central triazatruxene moiety (Scheme 1).

Published on 15 November 2018. Downloaded by University of Glasgow Library on 11/16/2018 11:25:17 AM.

Journal of Materials Chemistry C Accepted Manuscript

View Article Online
DOI: 10.1039/C8TC04231D

Published on 15 November 2018. Downloaded by University of Glasgow Library on 11/16/2018 11:25:17 AM.

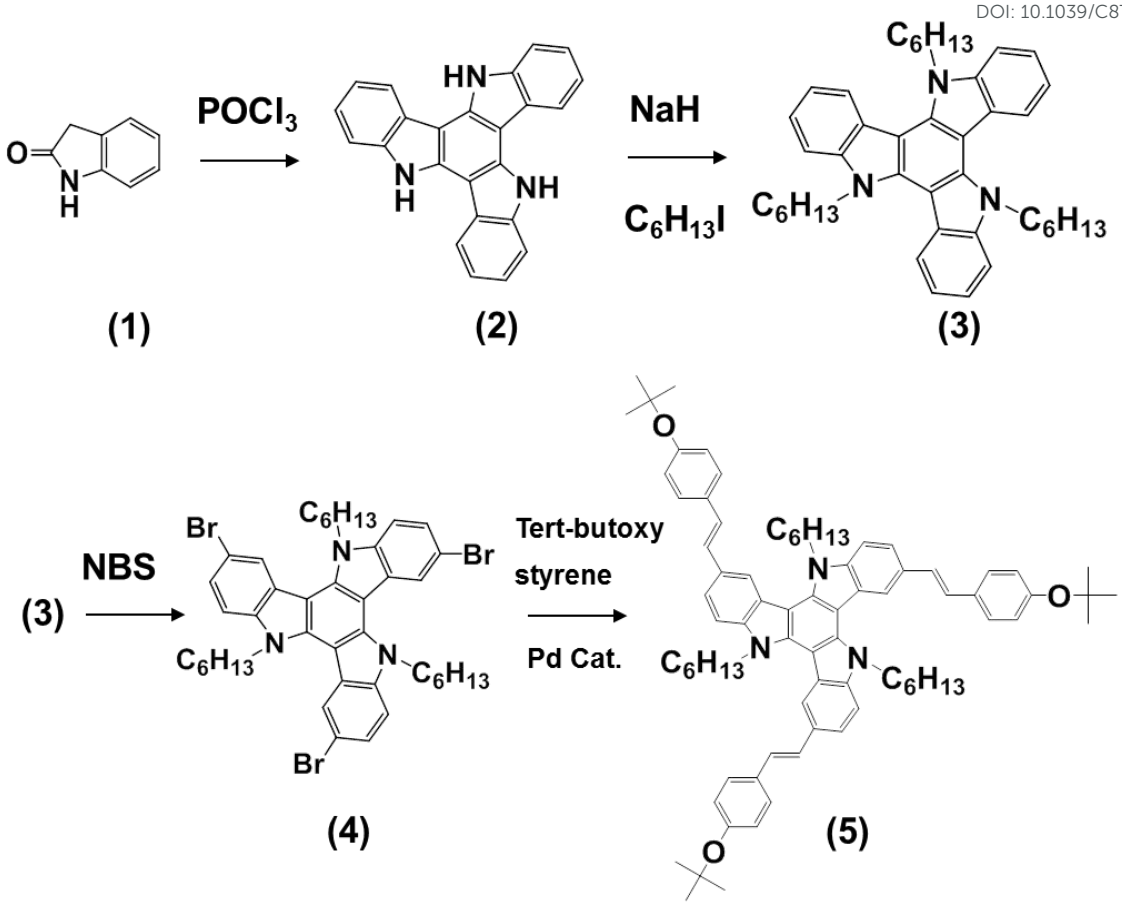

Scheme1. Synthesis of TAT-^{t}BuSty.

Synthesis and characterization data of **(2)**, **(3)** and **(4)** are included in the ESI (S2-S3). TAT-^{t}BuSty **(5)** has been characterized using ^{1}H-NMR, ^{13}C-NMR, high resolution mass spectrometry, UV-Vis spectroscopy and melting point analysis. Five nuclear environments for protons resonating in the aromatic region can be identified in the ^{1}H-NMR spectrum. Three of these integrate to 3H each and correspond to the protons of the triazatruxene core with the expected multiplicity of a singlet and two doublets. The other two resonances have the correct multiplicity expected from the protons of the *tert*-butoxy styrene phenyl ring; i.e. two doublets. However, the integration of 8H each is greater than the 6H for each resonance expected. We ascribe this to overlap with the methylene protons of the vinyl group which, are otherwise absent from the spectrum. Five nuclear environments for methyl protons are present in the molecule as is expected from the molecular structure. A multiplet resonating at 4.99-4.92ppm and integrating to 6H corresponds to the methyl protons bonded to the α-carbon of the hexyl chain linked to each nitrogen of the triazatruxene. The remaining peaks resonating in the methyl region consist of a doublet resonating at 2.02ppm integrating to 6H, two overlapping multiplets from 1.43-1.22ppm integrating to 47H and a triplet corresponding to the remaining methyl CH_2 protons in the β, γ, δ and ε positions of the hexyl chain with the methyl groups of the *tert*-butyl group. Finally, the multiplet at 0.87-0.80ppm integrating

Journal of Materials Chemistry C Accepted Manuscript

View Article Online
DOI: 10.1039/C8TC04231D

Published on 15 November 2018. Downloaded by University of Glasgow Library on 11/16/2018 11:25:17 AM.

to 9H corresponds to the CH_3 end of the hexyl chain. The ^{13}C-NMR spectrum shows thirteen resonances in the aromatic region and eight for the methyl group region. This is in line with the expected number of carbon environments for this molecule. Furthermore, the downfield shift of resonances at 78.49ppm corresponds to the α-carbon of the *tert*-butoxy group de-shielded by the electronegative oxygen, with the α-carbon of the hexyl chain resonating at 46.94ppm due to the de-shielding effect of the triazatruxene nitrogen. High resolution mass spectrometry using positive electrospray shows M^+ of 1120.7283 a.m.u. and a match for the theoretical isotope profile predicted for this molecule.

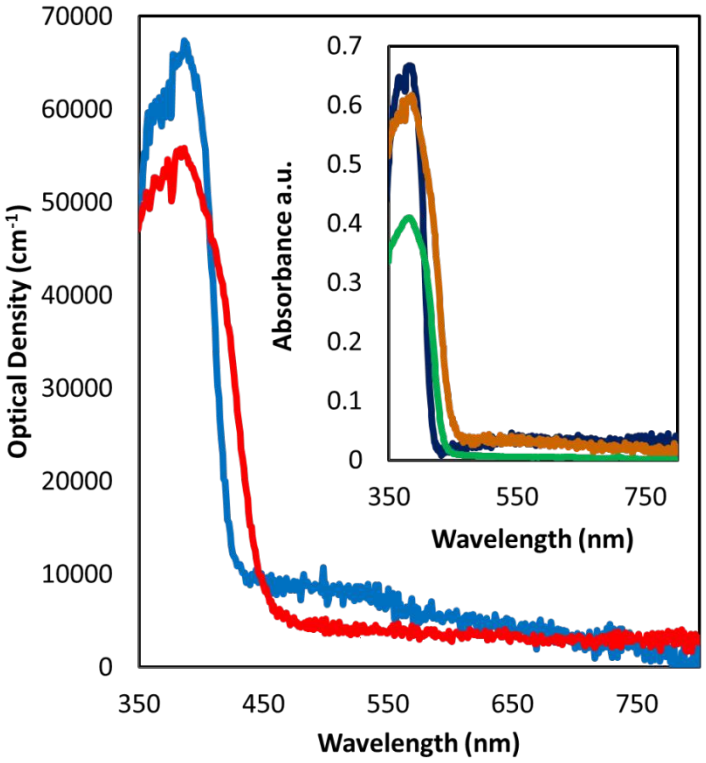

Figure 2. UV-vis spectra for a 100-nm-thick TAT-^{t}BuSty thin film (red line) and a 100-nm-thick spiro-OMeTAD (blue line). Thin films were spin coated onto glass substrates from chlorobenzene solution. Onset is Absorbance spectrum for 1mM TAT-^{t}BuSty in chlorobenzene solution (green line), a 100nm TAT-^{t}BuSty thin film (yellow line) and a 100 nm spiro-OMeTAD thin film (navy line).

The onset of Figure 2 shows that TAT-^{t}BuSty has a solution λ_{max} of 383nm with extinction coefficient of 4.645 x 10^4 M^{-1} cm^{-1} which is *ca.* ⅔ that of spiro-OMeTAD (ε = 7.00 x 10^4 M^{-1} cm^{-1})[16]. Lower extinction coefficients for HTMs can be important since it can be used to optimise the transparency of the HTM which is important for maximising photon absorption in device architectures where

Journal of Materials Chemistry C Accepted Manuscript

View Article Online
DOI: 10.1039/C8TC04231D

Published on 15 November 2018. Downloaded by University of Glasgow Library on 11/16/2018 11:25:17 AM.

light is incident through the HTM. The solution data also show a slight red shift (Abs_{onset} = 440nm, λ_{max} = 383nm) for TAT-^{t}BuSty compared with the closest literature structure, K131 (Abs_{onset} = 380nm, λ_{max} = 330nm)[14]. These bathochromic shifts are attributed to the additional conjugation from the three double bonds connecting the *tert*-butoxy ligands to the triazatruxene core in TAT-^{t}BuSty compared to single C-C bonds in the equivalent positions of K131. A bathochromic shift of *ca.* 20nm (460nm to 440nm) is also observed for the Abs_{onset} of a thin film of TAT-^{t}BuSty *vs* solution. Whilst this has not been reported before for truxene or triazatruxene PSC HTMs, it has been observed for other HTMs and has been attributed to intermolecular interactions between adjacent molecules[17, 18]. The Abs_{onset} of TAT-^{t}BuSty is also red-shifted 40nm compared to spiro-OMeTAD (460 vs 420nm). We ascribe this to increased intermolecular interactions of the planar TAT-^{t}BuSty compared to the spiro-OMeTAD which contains a spiro centre to reduce intermolecular stacking interactions. This, when compared with the device data for TAT-^{t}BuSty, suggest that stacking may be less of a problem than previously thought although X-ray diffraction analysis of spiro-OMeTAD and TAT-^{t}BuSty films shows that both samples do not exhibit any additional diffraction peaks compared with the FTO substrate (S9 in the ESI).

Contact angle measurements for water droplets on films of TAT-^{t}BuSty and spiro-OMeTAD tape cast from CH_2Cl_2 were measured (S6 in the ESI). Increased hydrophobicity is observed for TAT-^{t}BuSty with a contact angle at 83.7° c.f. 70.1° spiro-OMeTAD and may be due to hydrophobic alkyl chains and tert-butyl groups. The contact angle for TAT-^{t}BuSty is comparable to those reported for truxene and triazatruxene HTMs[15,19] with the data shown for spiro-OMeTAD being consistent with literature measurements[20].

Cyclic and square wave voltammograms of compounds **(3)** and TAT-^{t}BuSty **(5)** were recorded to estimate the reversibility and to determine the ionization potential (IP) and electron affinity (EA) of these molecules, respectively (S7 ESI). Cyclic voltammetry of the alkylated triazatruxene core **(3)** shows a *pseudo*-reversible oxidation wave at 0.40V (∂ = 65mV) whilst **(5)** shows a similar *pseudo*-reversible oxidation wave at 0.32V (∂ = 83mV). The corresponding IPs, estimated from square wave voltammetry, are −5.2 and −5.1eV, respectively. The reduction waves of both compounds are irreversible and their EAs estimated from square wave voltammetry correspond to −3.2 and −3.3eV, respectively.

By analyzing its electrical performance parameters, such as field-effect mobility, threshold-voltage and subthreshold swing, a thin-film transistor (TFT) can be used as a powerful tool to elucidate the properties of charge transport and the distribution of trap states in a semiconducting

Journal of Materials Chemistry C Accepted Manuscript

View Article Online
DOI: 10.1039/C8TC04231D

material[21]. To further the understanding of our HTM TAT-^{t}BuSty, we fabricated top-gate bottom-contact (TG-BC) TFTs using spiro-OMeTAD and TAT-^{t}BuSty as the active materials, and the details of the transistor fabrication can be found in the experimental section. Charge transfer characteristics (Fig. 3) were measured for spiro-OMeTAD and TAT-^{t}BuSty devices, respectively, and the key performance parameters are summarised in Table 1. It is clear in the current-voltage (I-V) characterisation (Fig. 3) that TAT-^{t}BuSty possesses a better transporting behaviour than spiro-OMeTAD as a higher channel current level (i.e. drain current, I_D) and no hysteresis were observed in the I-V sweeps. Regarding the pronounced I-V hysteresis shown in spiro-OMeTAD based transistors, there could exist a significant number of trap sites within the spiro-OMeTAD's film since clockwise hysteresis loops were observed. The latter is opposite to a usual counter-clockwise hysteresis loop that often refers to trap sites at semiconductor/dielectric interfaces[22]. However, it is important to note that this clockwise behavior is less likely to be caused by the existence of mobile ions within the gate dielectric since an inert Teflon-based material was used in this work. Besides, there was no observation of hysteresis while operating a TAT-^{t}BuSty transistor. If the gate dielectric took part in such hysteresis behaviours, both spiro-OMeTAD and TAT-^{t}BuSty based devices should see the same hysteresis loop during their operation. Regarding the transistor performance parameters (Table 1), the intrinsic TAT-^{t}BuSty based transistors also exhibit lower threshold-voltage (V_{TH}), higher linear field-effect mobility (μ_{LIN}), lower subthreshold swing (S.S.) and a lower trap-state density (D_{trap}). As such, in addition to the low-manufacturing cost, these advantageous properties obtained from the TAT-^{t}BuSty molecule based TFTs indicate that TAT-^{t}BuSty could be a highly suitable hole-transporting material for the replacement of spiro-OMeTAD in large-scale perovskite-based solar panel applications.

Published on 15 November 2018. Downloaded by University of Glasgow Library on 11/16/2018 11:25:17 AM.

Journal of Materials Chemistry C Accepted Manuscript

View Article Online
DOI: 10.1039/C8TC04231D

Published on 15 November 2018. Downloaded by University of Glasgow Library on 11/16/2018 11:25:17 AM.

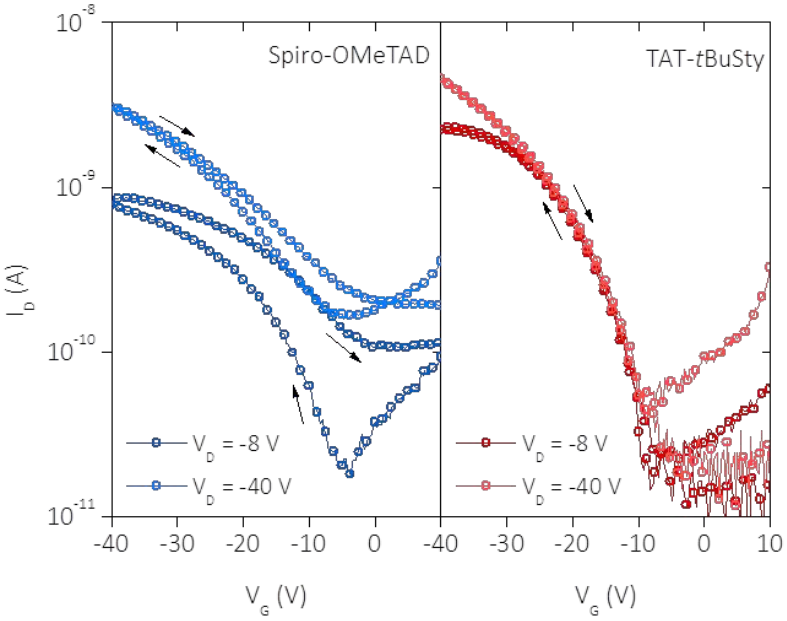

Figure 3. Transfer current-voltage characteristics for spiro-OMeTAD and TAT-*t*BuSty based TG-BC TFTs.

Table 1. Summary of key transistor performance parameters, including threshold voltage (V_{TH}), linear field-effect mobility (μ_{LIN}), forward-sweep subthreshold swing (FW S.S.), backward-sweep subthreshold swing (BW S.S.), forward-sweep trap density ($D_{trap, FW}$) and backward trap density ($D_{trap, BW}$).

HTM	VTH (V)	μ_{LIN} (cm^2/Vs)	FW S.S. (V/dec)	BW S.S. (V/dec)	$D_{trap, FW}$ ($x10^{12}$ $eV^{-1}cm^{-2}$)	$D_{trap, BW}$ ($x10^{12}$ $eV^{-1}cm^{-2}$)
Spiro-OMeTAD	-11.1	$2.9x10^{-5}$	13.3	17.7	7.2	9.6
TAT-*t*BuSty	-8.7	$5.1x10^{-5}$	3.3	3.4	1.7	1.8

We assessed TAT-*t*BuSty as a HTM in planar heterojunction PSCs [with a device structure, fluoride-doped tin oxide (FTO)/SnO_2/perovskite $Cs_{0.17}FA_{0.83}Pb(I_{0.9}Br_{0.1})_3$/HTM/Au]. The current density-voltage (*J-V*) characteristics (Fig. 4a) were measured under a simulated air mass (AM) 1.5 and 100 mW cm^{-2} of sunlight. As determined from the forward bias (FB) to short-circuit (SC) current-voltage scan, the device using the TAT-*t*BuSty shows a champion efficiency of 20.3% with a J_{sc} of 22.1 mA cm^{-2}, a V_{oc} of 1.15 V and a FF of 0.80. We also show the external quantum efficiency (EQE) spectra for representative TAT-*t*BuSty and spiro-OMeTAD devices (Fig. 4b). The TAT-*t*BuSty device shows a similar EQE spectrum to the spiro-OMeTAD device, with an integrated current density of 21.2 mA

Journal of Materials Chemistry C Accepted Manuscript

View Article Online
DOI: 10.1039/C8TC04231D

Published on 15 November 2018. Downloaded by University of Glasgow Library on 11/16/2018 11:25:17 AM.

cm^{-2}, which is in close agreement with the *J-V* scan. Due to the hysteretic behaviour of PSCs, we performed a stabilized efficiency measurement to accurately access the performance of the device (Fig. 4c). By holding the cells at a fixed maximum power point forward bias voltage, we measured the power output over time, reaching a stabilized efficiency of 19.4%. We also show a distribution of the performance parameters (Fig. 4d) for the devices tested in this study. On the whole, the TAT-^{t}BuSty and spiro-OMeTAD devices show comparable performances. Furthermore, a comparison with the current-voltage parameters of TAT-^{t}BuSty with the next best performing truxene and triazatruxenes reported to date (S8) shows that, to the best of our knowledge, TAT-^{t}BuSty produces the highest efficiency perovskite devices reported in the literature for this new family of HTMs.

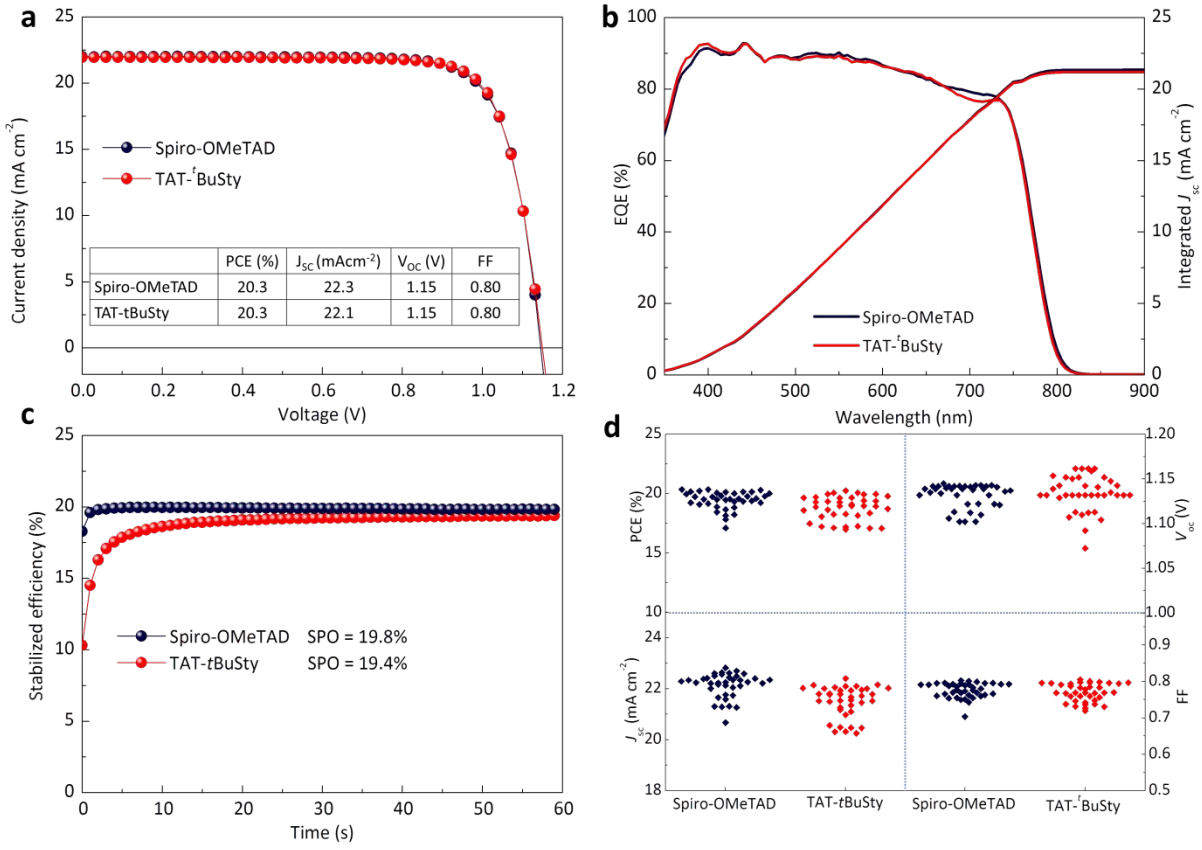

Figure 4. Device performance using Spiro-OMeTAD and TAT-*t*BuSty as HTM layers. (a) *J–V* characteristics of optimized perovskite solar cells with FTO/SnO_2/perovskite/HTM/Au device structure. (b) External quantum efficiency (EQE) spectra. (c) Stabilized power output (SPO) of the champion cells, determined by holding the cell at a fixed voltage near the maximum power point on the *J–V* curve for 60 s. (d) Distribution of PCE, V_{oc}, J_{sc} and FF for devices tested in this work.

Journal of Materials Chemistry C Accepted Manuscript

View Article Online
DOI: 10.1039/C8TC04231D

Published on 15 November 2018. Downloaded by University of Glasgow Library on 11/16/2018 11:25:17 AM.

Differential scanning calorimetry of TAT-^{t}BuSty (S5) was used to measure a small endotherm at 38^{o}C and an exotherm at 54^{o}C on the first heating cycle. By comparison, endothermic and exothermic peaks are observed at 154^{o}C and 245^{o}C for spiro-OMeTAD. The endotherm at 154^{o}C has not been reported for spiro-OMeTAD before but could be associated with crystallite formation. However, the exotherm at 245^{o}C is consistent with literature reports for the melting point of this material[23]. Correspondingly, a melting temperature of 54^{o}C is observed for TAT-^{t}BuSty. Thermal analysis data for other triazatruxene and truxene HTMs has been reported in the literature[14,15,19,24,25]. A melting point of 333^{o}C was reported for 5,10,15-tribenzyl-5H-diindolo[3,2-a:3′,2′-c]-carbazole (TBDI)[24]. Nazeeruddin *et al.* reported thermal stability data for a series of triazatruxenes; (K122), (K131), (K133) and (K145)[14] with full names in S10. The authors state that the decomposition temperature of the lowest molecular weight HTM of this series, K122 started at 439^{o}C, with K131, K133 and K145 having decomposition temperatures > 440^{o}C[14]. It was also reported that these HTMs do not exhibit melting behaviour with the authors suggesting that they are amorphous solids. Thermal analysis of (K122) is also reported in reference [25]. The authors use the acronym of HMDI for the HTM and report decomposition and glass transition temperatures of 350 and 1^{o}C, respectively. The decomposition temperature reported is *ca.* 90^{o}C lower than that reported in [14] for this HTM. Another HTM, "HPDI" is also reported in [25]. This material has a molecular weight of *ca.* 200 mass units higher than HMDI with the donor ligands attached to the nitrogen atoms of the triazatruxene centre. The authors reported an increase of thermal decomposition and glass transition temperatures to *ca.* 450 and 36^{o}C respectively. Li, Jen and Chen *et. al.* reported that truxene HTM (TruxOMeTAD – full name in S10) is thermally stable up to 400^{o}C and exhibits a melting point at 212^{o}C with the authors suggesting that it is a crystalline solid[19]. The authors also report that an annealing treatment at 150^{o}C for 10 min in an inert atmosphere was required for device optimization using this HTM. Finally, Su *et. al.* report a thermal decomposition temperature of *ca.* 420^{o}C and T_g values of 98^{o}C and 125^{o}C for HTMs (SP11) and (SP12) respectively[15]. This brief overview of thermal analysis data reported in the literature suggests that increasing the molecular weight of triazatruxene HTMs increases thermal decomposition temperatures. However, a correlation between molecular weight with melting and T_g is not clear. For example, the molecular weight of SP11 is *ca.* 300 mass units higher than SP12 but the T_g is *ca.* 25^{o}C lower[15]. It is clearly apparent, that future improvements in the TAT-^{t}BuSty which we report here, should include increasing its melting temperature to enable long term, thermally stable PSCs.

Film stability

Journal of Materials Chemistry C Accepted Manuscript

View Article Online
DOI: 10.1039/C8TC04231D

Published on 15 November 2018. Downloaded by University of Glasgow Library on 11/16/2018 11:25:17 AM.

To test thermal stability films of spiro-OMeTAD and TAT-^{t}BuSty were subjected to thermal cycling (30 min at 80°C followed by 30 min at ambient) and compared to films left in air. The digital imaging data (S11a) show no significant change in the optical appearance of spiro-OMeTAD or TAT-^{t}BuSty films either over 7 heating (30 min, 80°C) and cooling (30 min, ambient air) cycles or when held in ambient air. The red, green, blue (RGB) colour analysis of these films (S11b) is in agreement with this. Both films show green and red components which are stable between 240 and 245 units and at *ca.* 235 units, respectively. Whilst the blue components are also stable, the spiro-OMeTAD film exhibits 225 units compared to 215 units for TAT-^{t}BuSty in line with the slight yellow colour for TAT-^{t}BuSty.

A comparison of the UV-vis data for these films after air exposure or heat cycling (S11c) show little change in either the spiro-OMeTAD or TAT-^{t}BuSty films from *ca.* 450 nm to 800 nm. However, in general, there is an increase in transmittance for both spiro-OMeTAD and TAT-^{t}BuSty films below 450 nm. This is ascribed to oxidation of the films which is well known for spiro-OMeTAD and which is key for it to operate as an HTM[26]. Importantly for TAT-^{t}BuSty, there is no significant difference in the data between the room temperature controls and the heat cycled films suggesting that, despite its low T_g, TAT-^{t}BuSty appears to be stable to thermal cycling.

Previously, Admad et al demonstrated that perovskite solar cells with a HTM having a very low Tg (~1^{o}C) showed good thermal stability. [25] We note that Tg is a measure of mechanical rather than thermal stability. Below the Tg, the HTM film is harder but brittle and so is potentially fragile but, above the Tg, the film will be more pliable. Thus, it can be argued that a high Tg HTM will be less adhesive and more likely to delaminate whilst a lower Tg HTM will be more adhesive and easier to deposit by melt processing. However, in either case the Tg does not directly indicate to either thermal or radiation stability. Instead these parameters are related to bond strengths, and light absorption and photochemical primary processes (e.g. homolytic bond breakage versus energy dissipation), respectively. Based on our thermal cycling study, we do not observe decomposition or any other negative effects for this new HTM compared to spiro-OMeTAD when cycled repeatedly between ambient and 80°C. Understanding low Tg HTMs at elevated temperatures in perovskite solar cells and its potential compatibility with flexible solar cells is a subject of ongoing study.

Cost analysis

S4.4 (ESI) shows a cost and yield summary for the ligand and reaction required for attaching the donor groups to prepare the high performance truxene and triazatruxene HTMs. The data show that the *tert*-butoxystyrene used as the donor ligand in TAT-^{t}BuSty is *ca.* ten times cheaper than the

Journal of Materials Chemistry C Accepted Manuscript

View Article Online
DOI: 10.1039/C8TC04231D

Published on 15 November 2018. Downloaded by University of Glasgow Library on 11/16/2018 11:25:17 AM.

donor ligands used to prepare the HTMs (S4.4). In addition, this cheaper ligand can be incorporated into the final molecule in higher yield under more forgiving reaction conditions. Thus, the Heck coupling reaction is completed in higher yield i.e. 95% by comparison to the highest yield of 86% reported for the Suzuki coupling reaction used to make SP-12[15]. Furthermore, TAT-*t*BuSty is simpler to purify than the other HTMs because this reaction involves adding a liquid starting material (*tert*-butoxystyrene) to a solid, **(4)**, to form a solid product. In practice, this enables excess liquid to be used to convert all of the solid. Then any excess liquid reactant can easily be recovered from the crude product by re-crystallisation or washing with solvent making purification much cheaper and simpler. By comparison, the final coupling reaction to synthesize the other HTMs in S4.4 [ESI] are prepared by reacting a solid with a solid to form a solid product, and therefore careful column chromatography is required to obtain a pure product which typically requires many litres of solvent per gram of pure product as is reported for a 10g synthesis of spiroxanthene HTM, SFX[27]. A cost analysis model for the synthesis of small molecule HTMs has been reported by Oesdach and Bulović [28]. Decampo *et. al.* have used this model to calculate the cost of synthesis of spiro-OMeTAD as \$112.05 g^{-1} [12]. To the best of our knowledge, two of the lowest cost HTMs reported in the literature are \$9.57 g^{-1} for EDOT-OMeTPA[12] and *ca.* \$15.78 g^{-1} for spiroxanthene SFX[27]. The lower cost of these materials by comparison to spiro-OMeTAD is due to fewer reactions steps, lower cost starting materials and less complex purification procedures required during the syntheses. We have used the same cost model to calculate the cost of TAT-*t*BuSty following synthesis route 1 (S4) as \$69.90 g^{-1}. By comparison, SP12 *i.e.* the next best performing triazatruxene HTM would cost \$93.60 g^{-1} following the synthesis procedure reported in[15]. In line with above, the increased cost of synthesis for SP12 is due to use of a more expensive paramethoxybenzene boronic acid ligand (10x the cost of *tert*-butoxystyrene) and more complicated column chromatography for purification requiring more solvent so the purification cost is double that for TAT-*t*BuSty. This indicates that the final reaction step for TAT-*t*BuSty is \$20.64 g^{-1} *vs* \$44.30 g^{-1} for SP12. TAT-*t*BuSty is therefore 24% cheaper to make than the next best performing triazatruxene reported in the literature. Synthesis of TAT-*t*BuSty *via* route 2 (S4.3) which involves alkylation of bromoisatin, followed by reduction to the oxindole, cyclisation to form the triazatruxene and finally a Pd-catalysed Heck coupling reaction to attach the ligand would further decrease the cost to *ca.* \$47 g^{-1}. The cost could be further decreased by recycling the CH_2Cl_2 required for the silica plug during the purification of the cyclized triazatruxene and by using a Pd acetate catalyst during the final coupling reaction. This decreases the quantity of organic waste produced which is important for synthesis of organic materials on a larger scale. This would also decrease the overall cost of synthesis by *ca.* \$10-\$15 g^{-1} to *ca.* \$3732

Journal of Materials Chemistry C Accepted Manuscript

View Article Online
DOI: 10.1039/C8TC04231D

Published on 15 November 2018. Downloaded by University of Glasgow Library on 11/16/2018 11:25:17 AM.

g^{-1}, which is *ca.* double the cost of spiroxanthenes. Thus, TAT-^{t}BuSty is amongst the lowest cost small molecule organic HTMs when accurate cost models for the synthesis are used. The contribution of the HTM to the overall cost for a perovskite module can be considered in the context of Lipomi and Burke[29] refer to the work of Lewis on Nocera who state that a solar energy conversion system should cost no more than \$10 m^{-2} to be competitive with fossil fuels for primary energy. Decampo *et. al.* have estimated that using EDOT-OMeTPA as HTM in a perovskite device, would lead to a contribution of 0.004 \$ W^{-1} from the HTM with a target module cost of 0.5 \$ W^{-1}. Slot die coating would minimize HTM material usage as there is *ca.* 10% wastage c.f. *ca.* 90% material waste using spin coating. This is less than 1% of the total module target cost. Synthesis of TAT-^{t}BuSty *via* route 2 (S4.3) with recycling of the purification solvent would cost *ca.* 3.5 times that of EDOT-OMeTPA. This means that TAT-^{t}BuSty would contribute *ca.* 0.015 \$ W^{-1} which is 3.5% of the module cost. However, TAT-^{t}BuSty has been used to prepare devices with over double the overall power conversion efficiency *vs* the report of EDOT-OMeTPA. In contrast, the cost of *ca.* \$112.05 g^{-1} for spiro-OMeTAD, would contribute to about 10% of the overall module cost.

Conclusions

We have synthesized a new HTM TAT-^{t}BuSty with inexpensive raw materials and greatly simplified the production of a high quality HTM. We first introduce a synthetic strategy of reacting a liquid precursor with a solid precursor to form the solid HTM product, which greatly simplifies the purification process and reduces the fabrication costs. PSC devices with the TAT-^{t}BuSty HTM shows a respectable efficiency of 20.3% which can match spiro-OMeTAD for performance in perovskite devices. Furthermore, we estimate that the cost for spiro-OMeTAD is about 10% of the module cost, while this can be significantly reduced to 3.5% when using the TAT-^{t}BuSty. Our work demonstrates that the TAT-based HTMs can be promising organic interlayers for efficient perovskite single-junction, and potentially all perovskite tandem cells. The considerably lowered costs and simplified synthesis and purification processes would offer great opportunity for up-scaling PSCs and flexible optoelectronics.

Experimental

Instrumentation and chemicals

All chemicals and solvents were purchased from Aldrich and used as supplied. NMR spectra were recorded on a Bruker AC400 instrument operating at 400 MHz for ^{1}H and 101 MHz for ^{13}C. Chemical shifts for ^{1}H and ^{13}C (δ) are given in ppm relative to $(CH_3)_4Si$. High resolution mass spectrometry

Journal of Materials Chemistry C Accepted Manuscript

View Article Online
DOI: 10.1039/C8TC04231D

data was obtained using recorded using positive electrospray at the EPSRC National Mass Spectrometry Service at the University of Swansea.

Cyclic voltammetry was recorded on HTMs (0.1 mM (**3**) and 0.1 mM (**5**)) at 25 ºC in N_2-saturated anhydrous CH_2Cl_2 using 0.1 M Bu_4NPF_6 as the supporting electrolyte. Measurements were performed using a CHI 440a electrochemical analyzer with a sweep rate 0.1 V s^{-1} using a three-electrode cell with a Pt (12.5 mm^2) working electrode, a Ag wire pseudo-reference electrode and a Pt wire counter electrode. Potentials are reported vs. Fc/Fc^+ ($E_{1/2}$= 0.308 V vs. Ag wire) and are adjusted to 0V. The corresponding electron affinities and ionization potentials are calculated relative to the Fc/Fc^+ redox couple (–4.8 eV) using squarewave voltammetry.

TG-BC TFTs were fabricated on glass substrates. The substrates were cleaned with acetone and isopropanol (IPA) in a sonication bath for 10 min for each step. 40-nm thick Au source and drain electrodes (channel width/length: 1000 μm/30 μm) were evaporated through shadow masks under vacuum, before being treated with a work function modifier pentafluorothiophenol (PFBT) self-assembled monolayer (SAM). For the SAM treatment, the substrates were submerged in a 5 mmol L^{-1} PFBT in IPA solution for 60 min. Upon completion of the SAM treatment, the substrates were rinsed with large amount of IPA to remove excessive unbonded PFBT and then blow-dried with N_2. The HTMs were deposited from a solution *via* spin coating at 2000 rpm for 30 s in a N_2 atmosphere. Following semiconductor depositions, a Teflon based material (AF2400, Dupont) dissolved in a Fluorinert™ electronic liquid (FC-43, 3M) at a concentration of 25 mg/mL and used as the gate dielectric was deposited *via* spin cast (1000 rpm, 30 s) to produce a ~330 nm thick dielectric layer, which was then annealed for 10 min at 40 °C in N_2. The TFTs were completed by thermal evaporation of 50-nm thick Al gate electrodes through shadow masks under high vacuum. Linear field-effect mobility was calculated using gradual-channel approximation[30]:

$$\mu_{LIN} = \frac{L}{W\, C_i\, V_D}\left(\frac{\partial I_{D,\,LIN}}{\partial V_G}\right)$$

Trap density was evaluated from the following equation[31]:

$$D_{trap} = \frac{C_i}{e^2}\left(\frac{e \times S.S.}{kT(10)} - 1\right)$$

Fabrication of perovskite solar cell devices:

Electron-transporting layer: 0.05 M $SnCl_4 \cdot 5H_2O$ (Sigma) was first dissolved in anhydrous IPA (Sigma) and stirred for 30 min at room temperature. The solution was deposited on cleaned FTO substrates with 3000 rpm spin rate for 30 s, followed by pre-drying at 100ºC for 10 min and then heat-treated at 180ºC for 1 h. The films were then treated using chemical bath deposition method, as described

Published on 15 November 2018. Downloaded by University of Glasgow Library on 11/16/2018 11:25:17 AM.
Journal of Materials Chemistry C Accepted Manuscript

View Article Online
DOI: 10.1039/C8TC04231D

Published on 15 November 2018. Downloaded by University of Glasgow Library on 11/16/2018 11:25:17 AM.

elsewhere[32]. 500 mg urea was dissolved in 40 ml deionized water, followed by the addition of 10 ml mercaptoacetic acid (Sigma) and 0.5 ml HCl (VWR; 37 wt%). Finally, $SnCl_2 \cdot 2H_2O$ (Sigma) was dissolved in the solution at 0.002 M and stirred for 2 min. The deposition was made by putting the substrates vertically in a glass container filled with the above solution, in a 70°C oven for 3 h. The treated substrates were rinsed in a sonication bath of deionized water for 2 min, dried in a stream of N_2 and annealed for 1 h at 180°C.

Perovskite absorber layer: $FA_{0.83}Cs_{0.17}Pb(I_{0.9}Br_{0.1})_3$ perovskite precursor solution were dissolved in a 4 : 1 (v : v) mixture of anhydrous DMF : DMSO (Sigma) to obtain a stoichiometric solution with desired composition using precursor salts: formamidinium iodide (FAI; Dyesol), caesium iodide (CsI; Alfa Aesar), lead iodide (PbI_2; TCI), lead bromide ($PbBr_2$; TCI). The concentration was 1.4 M. The solution was made in a N_2-filled glovebox and kept stirring overnight at room temperature. The perovskite precursor solution was deposited through a two-step spin coating program (10 s at 1000 rpm and 32 s at 6000 rpm) with dripping of chlorobenzene (Sigma) as anti-solvent during the second step, 8 s before the end. All the films annealed at 100°C for 60 min.

Hole-transporting layer: TAT-*t*BuSty was dissolved in chlorobenzene (35 mM). Sprio-OMeTAD (Borun Technology 99.8%) was dissolved in in chlorobenzene (70 mM). 10.7 mol% of *tert*-butylpyridine (Sigma; tBP) and 25 mol% tris(bis(trifluoromethylsulfon-yl)imide) (Sigma; Li-TFSI) (from a 1.8 M stock solution in acetonitrile) were added as additives. The final HTM solutions were spin-coated onto the perovskite layers at 2000 rpm for 45s.

Electrode deposition: 80 nm gold electrodes were thermally evaporated under vacuum of $\sim 5 \times 10^{-6}$ Torr, at a rate of ~ 1 Å s^{-1}. Note that the temperature of the vacuum chamber was controlled (< 40°C) during the evaporation of the metal electrodes as higher temperature will cause possible degradation of perovskite films.

Current–Voltage Measurements: The current density–voltage (*J-V*) curves were measured (2400 Series SourceMeter, Keithley Instruments) under simulated AM 1.5G sunlight at 100 mW cm^{-2} irradiance generated by an Abet Class AAB sun 2000 simulator, with the intensity calibrated with an NREL calibrated KG5 filtered Si reference cell. The mismatch factor was calculated to be less than 5%. The active area of the solar cell is 0.0919 cm^{-2}. The forward *J–V* scans were measured from forward bias (FB) to short circuit (SC) and the backward scans were from short circuit to forward bias, both at a scan rate of 380 mV s^{-1}. A stabilization time of 5 s at forward bias of 1.4 V under illumination was done prior to scanning.

Journal of Materials Chemistry C Accepted Manuscript

View Article Online
DOI: 10.1039/C8TC04231D

X-ray Diffraction Measurements: X-ray diffraction measurements were carried out using a Bruker D8 Discover with Da Vinci software with a copper source (40kV, 40mA). Tests were carried out using 0.05 2Theta increments with a 0.5 second step time.

Film Stability Testing: Fluoride-doped SnO_2 (FTO) coated glass substrates (Solaronix) were ultrasonicated in acetone followed by O_2 plasma cleaning. Chlorobenzene solutions of TAT-^{t}BuSty (35 mM) or spiro-OMeTAD (Borun Technology 99.8%) i (70 mM) were prepared each containing 10.7 mol% of *tert*-butyl pyridine (Sigma) and 25 mol% tris(bis(trifluoromethylsulfon-yl)imide (Sigma; Li-TFSI). The HTM solutions were spin-coated onto the glass at 2000 rpm for 45s. Both of the HTM layers were measured as *ca.* 90 nm with a DekTak profilometer. To measure HTM film stability, control samples were left in air at ambient temperature. A second set of films were heated to 80˚C for 30 min and then allowed to cool to ambient temperature for 30 min; this sequence made once heating cycle. After each cycle, the films were analysed by UV-visible spectrometry (Varian Cary 5000) and digital imaging using a Canon EOS 1100D camera (F-stop 29, exposure time 0.3s, ISO 100) in a Photosimile 200 lightbox. RGB data were extracted and analysed as described by Furnell *et al.*[33].

Synthesis

The preparation of 3,8,13-tribromo-5,10,15-trihexyl-10,15-dihydro-5H-diindolo[3,2-a:3',2'-c]carbazole is included in the ESI (S1) and uses the method published in [10].

Synthesis of TAT-^{t}BuSty (5)

3,8,13-tribromo-5,10,15-trihexyl-10,15-dihydro-5H-diindolo[3,2-a:3',2'-c]carbazole, **(4)** (0.5g, 0.78mmol) was dissolved in *N, N'*-dimethylacetamide (10ml) with tert-butoxystyrene (5equiv., 0.68g, 3.91mmol) with trans-di(m-acetato)bis[O-(di-o-tolylphosphino)benzyl]dipalladium(II) (0.045g, 0.15mmol) and Na_2CO_3 (0.25g, 2.5mmol) and the solution was stirred under N_2 at 130^{o}C for 24 h. After cooling, the solution was poured into distilled H_2O-CH_2Cl_2 (100ml, 1:1 v/v) and the mixture separated using a separating funnel. The organic layer was dried over anhydrous $MgSO_4$ and the solvent removed *in vacuo* before purification using a silica plug with *n*-hexane-CH_2Cl_2 (9:1 v/v) as an eluent and precipitation with MeOH poured into a solution in CH_2Cl_2 to give a yellow solid. Yield 95% 0.83g

^{1}H NMR (400 MHz, CD_2Cl_2) δ 8.28 (d, *J* = 8.0 Hz, 3H), 7.76 (s, 3H), 7.58 (m, 8H), 7.33 (d, *J* = 4.4 Hz, 3H), 7.07 (m, 6H), 5.02 – 4.90 (m, 8H), 2.02 (d, *J* = 6.1 Hz, 6H), 1.42-1.20 (m, 47H), 0.89 – 0.78 (m, 9H).

Published on 15 November 2018. Downloaded by University of Glasgow Library on 11/16/2018 11:25:17 AM.
Journal of Materials Chemistry C Accepted Manuscript

View Article Online
DOI: 10.1039/C8TC04231D

^{13}C NMR (101 MHz, CD_2Cl_2) δ 155.18, 141.44, 132.86, 128.93, 128.90, 128.24, 126.84, 126.63, 124.24, 121.62, 118.33, 112.50, 111.08, 78.49, 46.94, 31.42, 29.63, 28.65, 26.28, 22.45, 13.70. MS (FTMS +) $[M + H]^+$, calculated = 1120, $[M + H]^+$ observed = 1120, *m/e* Accurate Mass (FTMS +), reference compound: NH_4OAc, $[M + H]^+$, calculated = 1120.7290, $[M + H]^+$ observed = 1120.7283 UV-vis: λ_{max} = 383 nm (ε = 4.645 x 10^4 M^{-1} cm^{-1}). Melting point (DSC) = 54°C

Acknowledgements

We gratefully acknowledge funding from the EPSRC SPACE-modules for AC, EWJ, PG and ZW (EP/M015254/1), the Welsh Government for Sêr Cymru (PJH) NRN (CK), the European Commission and ERDF for SPARC II funding (LF and RA). We also thank the EPSRC UK National Mass Spectrometry Facility at Swansea University.

Supplementary material

Supporting Information. Characterisation spectra for **(5)** and synthesis details for all precursors in included. In addition, thermal analysis, electrochemical, contact angle data and cost analyses are also included. This material is available free of charge via the Internet at http://pubs.acs.org."

AUTHOR INFORMATION

Corresponding Author

Peter J. Holliman[†,*] Henry J. Snaith[‡,*] and Zhiping Wang[‡,*]

[†] College of Engineering, Bay Campus, Swansea University, Swansea, SA1 8EN, UK. [‡] Department of Physics, University of Oxford, Clarendon Laboratory, Parks Road, Oxford OX1 3PU, UK.

Funding Sources

We gratefully acknowledge funding from the EPSRC SPACE-modules for AC, EWJ, PG and ZW (EP/M015254/1), the Welsh Government for Sêr Cymru (PJH) NRN (CK), the European Commission and ERDF for SPARC II funding (LF and RA). We also thank the EPSRC UK National Mass Spectrometry Facility at Swansea University.

References

1 A. Kojima, K. Teshima, Y. Shirai and T. Miyasaka, *J. Am. Chem. Soc.*, 2009, **131**, 6050–6051.

2 M. M. Lee, J. Teuscher, T. Miyasaka, T. N. Murakami and H. J. Snaith, *Science*, 2012, **338**, 643–7.

Published on 15 November 2018. Downloaded by University of Glasgow Library on 11/16/2018 11:25:17 AM.

Journal of Materials Chemistry C Accepted Manuscript

View Article Online
DOI: 10.1039/C8TC04231D

Published on 15 November 2018. Downloaded by University of Glasgow Library on 11/16/2018 11:25:17 AM.

3 M. Liu, M. B. Johnston and H. J. Snaith, *Nature*, 2013, **501**, 395–8.

4 M. Saliba, T. Matsui, J.-Y. Seo, K. Domanski, J.-P. Correa-Baena, M. K. Nazeeruddin, S. M. Zakeeruddin, W. Tress, A. Abate, A. Hagfeldt and M. Grätzel, *Energy Environ. Sci.*, 2016, **9**, 1989–1997.

5 M. Saliba, S. Orlandi, T. Matsui, S. Aghazada, M. Cavazzini, J.-P. Correa-Baena, P. Gao, R. Scopelliti, E. Mosconi, K.-H. Dahmen, F. De Angelis, A. Abate, A. Hagfeldt, G. Pozzi, M. Graetzel and M. K. Nazeeruddin, *Nat. Energy*, 2016, **1**, 15017.

6 W. S. Yang, B. Park, E. H. Jung, N. J. Jeon, Y. C. Kim, D. U. Lee, S. S. Shin, J. Seo, E. K. Kim, J. H. Noh and S. Il Seok, *Science (80-.).*, 2017, **356**, 1376–1379.

7 J. T.-W. Wang, Z. Wang, S. Pathak, W. Zhang, D. W. DeQuilettes, F. Wisnivesky-Rocca-Rivarola, J. Huang, P. K. Nayak, J. B. Patel, H. A. Mohd Yusof, Y. Vaynzof, R. Zhu, I. Ramirez, J. Zhang, C. Ducati, C. Grovenor, M. B. Johnston, D. S. Ginger, R. J. Nicholas and H. J. Snaith, *Energy Environ. Sci.*, 2016, **9**, 2892–2901.

8 Z. Wang, D. P. McMeekin, N. Sakai, S. van Reenen, K. Wojciechowski, J. B. Patel, M. B. Johnston and H. J. Snaith, *Adv. Mater.*, 2017, **29**, 1604186.

9 Z. Wang, Q. Lin, F. P. Chmiel, N. Sakai, L. M. Herz and H. J. Snaith, *Nat. Energy*, 2017, **2**, 17135.

10 Z. Wang, Q. Lin, B. Wenger, M. G. Christoforo, Y. Lin, M. T. Klug, M. B. Johnston, L. M. Herz and H. J. Snaith, *Nat. Energy*, 2018, DOI：10.1038/s41560-018-0220-2.

11 http://www.nrel.gov/ncpv/images/efficiency_charg.jpg, .

12 M. L. Petrus, T. Bein, T. J. Dingemans and P. Docampo, *J. Mater. Chem. A*, 2015, **3**, 12159–12162.

13 I. W. Shen, M. C. McCairn, J. J. Morrison and M. L. Turner, *Macromol. Rapid Commun.*, 2007, **28**, 449–455.

14 K. Rakstys, A. Abate, M. I. Dar, P. Gao, V. Jankauskas, G. Jacopin, E. Kamarauskas, S. Kazim, S. Ahmad, M. Grätzel and M. K. Nazeeruddin, *J. Am. Chem. Soc.*, 2015, **137**, 16172–16178.

15 P. Y. Su, L. B. Huang, J. M. Liu, Y. F. Chen, L. M. Xiao, D. Bin Kuang, M. Mayor and C. Y. Su, *J. Mater. Chem. A*, 2017, **5**, 1913–1918.

16 U. B. Cappel, E. A. Gibson, A. Hagfeldt and G. Boschloo, *J. Phys. Chem. C*, 2009, **113**, 6275–6281.

17 S. Park, J. H. Heo, C. H. Cheon, H. Kim, S. H. Im and H. J. Son, *J. Mater. Chem. A*, 2015, **3**, 24215–24220.

18 J. Liu, Y. Wu, C. Qin, X. Yang, T. Yasuda, A. Islam, K. Zhang, W. Peng, W. Chen and L. Han, *Energy Environ. Sci.*, 2014, **7**, 2963–2967.

Journal of Materials Chemistry C Accepted Manuscript

View Article Online
DOI: 10.1039/C8TC04231D

Published on 15 November 2018. Downloaded by University of Glasgow Library on 11/16/2018 11:25:17 AM.

19 C. Huang, W. Fu, C.-Z. Li, Z. Zhang, W. Qiu, M. Shi, P. Heremans, A. K.-Y. Jen and H. Chen, *J. Am. Chem. Soc.*, 2016, **138**, 2528–2531.

20 T. Leijtens, T. Giovenzana, S. N. Habisreutinger, J. S. Tinkham, N. K. Noel, B. A. Kamino, G. Sadoughi, A. Sellinger and H. J. Snaith, *ACS Appl. Mater. Interfaces*, 2016, **8**, 5981–5989.

21 A. Salleo, *Mater. Today*, 2007, **10**, 38–45.

22 M. Egginger, S. Bauer, R. Schwödiauer, H. Neugebauer and N. S. Sariciftci, *Monatshefte fur Chemie*, 2009, 140, 735–750.

23 T. Malinauskas, D. Tomkute-Luksiene, R. Sens, M. Daskeviciene, R. Send, H. Wonneberger, V. Jankauskas, I. Bruder and V. Getautis, *ACS Appl. Mater. Interfaces*, 2015, **7**, 11107–11116.

24 L. Calió, C. Momblona, L. Gil-Escrig, S. Kazim, M. Sessolo, Á. Sastre-Santos, H. J. Bolink and S. Ahmad, *Sol. Energy Mater. Sol. Cells*, 2017, **163**, 237–241.

25 F. J. Ramos, K. Rakstys, S. Kazim, M. Grätzel, M. K. Nazeeruddin and S. Ahmad, *RSC Adv.*, 2015, **5**, 53426–53432.

26. W.H. Nguyen, C.D. Bailie, E.L. Unger, M.D. McGehee, J. Am. Chem. Soc., 2014, **136**, 10996-11001.

27 M. Maciejczyk, A. Ivaturi and N. Robertson, *J. Mater. Chem. A*, 2016, **4**, 4855–4863.

28 T. P. Osedach, T. L. Andrew and V. Bulović, *Energy Environ. Sci.*, 2013, **6**, 711–718.

29 D. J. Burke and D. J. Lipomi, *Energy Environ. Sci.*, 2013, **6**, 2053.

30 S. M. Sze and K. K. Ng, *Physics of Semiconductor Devices: Third Edition*, 2006.

31 Y. H. Lin, H. Faber, S. Rossbauer and T. D. Anthopoulos, *Appl. Phys. Lett.*, 2013, **102**, 193516.

32 E. H. Anaraki, A. Kermanpur, L. Steier, K. Domanski, T. Matsui, W. Tress, M. Saliba, A. Abate, M. Grätzel, A. Hagfeldt and J.-P. Correa-Baena, *Energy Environ. Sci.*, 2016, **9**, 3128–3134.

33. L. Furnell, P.J. Holliman, A. Connell, E.W. Jones, R. Hobbs, C.P. Kershaw, R. Anthony, J. Searle, T. Watson, J. McGettrick, *Sustainable Energy & Fuels*, 2017, **1**, 362-370.

Journal of Materials Chemistry C Accepted Manuscript